

Hierarchical annealing for synthesis of binary porous media images

Simon K. Alexander* and Edward R. Vrscay
Department of Applied Mathematics, University of Waterloo

Paul Fieguth
Department of Systems Design Engineering, University of Waterloo

Marios A. Ioannidis
Department of Chemical Engineering, University of Waterloo

The introduction of a hierarchical annealing algorithm addresses the very large computational costs associated with simulated annealing for the synthesis of binary porous media images. In real-world examples, the large configuration space of such models has led to disappointing performance of annealing approaches. We demonstrate orders-of-magnitude improvement compared to existing results, and discuss the inherent computational difficulties encountered with these types of approaches.

PACS numbers: 0.25.Ey, 02.70.-c, 42.30.Wb, 83.80.Nb **FIXME:** *check these*

I. INTRODUCTION

A great variety of porous media (see Figure 1) and composites have a random heterogeneous microstructure. The generation of 3D (or large 2D) replicas of such materials from limited (usually 2D) morphological information by stochastic methods is an intriguing problem of broad technological and scientific significance [27, 32]. The significance of this problem follows from the fact that the macroscopic properties (mechanical, transport, capillary and electromagnetic) of such materials cannot be predicted from knowledge of the volume fractions of the constituent phases alone. Instead, the geometry and topology of the convoluted 3D boundary surface separating the constituent phases must be accounted for.

From a practical standpoint, stochastic reconstruction from limited morphological information is linked directly to the computation of macroscopic properties of engineering materials from first principles. Much progress has been made in this direction. For example, efficient methods are now in place for computing elastic properties [7, 23], absolute permeability [14, 28, 29] and formation resistivity factor [2, 11, 14, 25] of fluid-saturated porous media, relative permeability and electrical conductivity under two-phase flow conditions [4], capillary pressure-saturation relationships [16], nuclear magnetic resonance properties [20] and adsorption/condensation characteristics [12] of porous solids from 3D digital representations of the microstructure. From a theoretical standpoint, stochastic reconstruction is a valuable tool for uncovering the information content of different descriptors of the morphology of a microstructure. Such knowledge is essential for selecting appropriately the morphological descriptors to be used as reconstruction constraints (i.e., the reconstruction model) for different classes of microstructures.

Two general approaches to stochastic reconstruction have been actively pursued in recent years. The first approach is

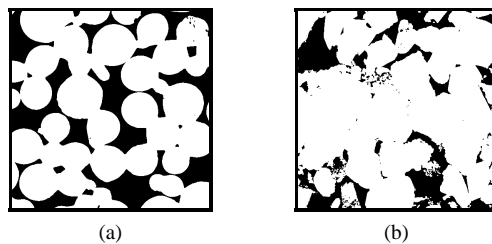


FIG. 1: Examples of binary porous media images a) sintered glass beads b) Berea sandstone.

based on the conditioning and truncation of Gaussian Random Fields [1, 5, 13, 24]. Though mathematically elegant and computationally very efficient, this method is model-dependent, since it cannot impose constraints other than the volume fraction and the two-point correlation function. This is a serious drawback, because first- (volume fraction) and second- (two-point correlation function) order statistics are, in general, insufficient for accurately reproducing the morphology of a microstructure [13, 22]. The second approach is based on simulated annealing (SA) [26, 31, 33]. This approach is model-independent, since in principle it can impose on the reconstruction process any type and number of morphological constraints (e.g., chord-length distributions). This advantage, however, is rapidly offset by the method's high demand for computational resources.

The presence of structure at multiple length scales is a well-established fact for natural porous rocks [e.g., [21] and references therein] and the need to account for it in stochastic reconstructions is beginning to receive recognition [18, 19]. For example, sandstones often contain significant amounts of microporosity in addition to inter-granular porosity, whereas carbonate rocks often contain vugs and solution channels of sizes much greater than the sizes of inter-particle pores. The presence of structure at multiple length scales creates unique challenges for the reconstruction process. To cope with models of rapidly increasing resolution[26], the efficiency of stochastic

*Electronic address: sk2alex@uwaterloo.ca

reconstruction algorithms must increase by orders of magnitude. New stochastic reconstruction algorithms must be developed that can accommodate and, if possible, capitalize on the scale-dependence of morphological descriptors.

In an important paper, Gidas [9] introduces the idea of renormalization to image processing contexts, and indeed addresses simulated annealing for the restoration of images in such a context. The current work is naturally related, but primarily differs in two important aspects. Firstly, Gidas discusses estimation, for example the denoising of an image. In such a problem, one wishes to construct an energy surface with the nominally *correct* image as a global minimum. In practice the problem is conditioned by the fact that in some sense we expect the correct image to be nearby in configuration space. In pure synthesis, by comparison, we are interested in exploring all minima of a complicated energy surface. Secondly, we are not only considering proper renormalizations of our configuration space, but rather we will be interested in the characteristics of a more general hierarchical approach.

In this paper, we propose a HSA algorithm for the reconstruction of random microstructures from limited morphological information. The hierarchical scheme allows large computational gains to be realized when applying this algorithm to models previously described in the literature [31], thus the focus of this work is on the computational benefits of this approach, as applied to *existing* models. Although it is natural to ask about the capabilities of such an approach to proposing *new* models, this question is the focus of ongoing research and lies beyond the scope of this paper.

II. RANDOM FIELDS, SIMULATED ANNEALING

We will model our porous media images as realizations of a Markov/Gibbs random field. Hence for synthesis of images from this (prior) model, we wish to sample a density:

$$\pi_\beta(x) = \frac{e^{-\beta\mathcal{E}(x)}}{Z_\beta} . \quad (1)$$

Here x denotes the image (i.e. current configuration), where $\beta = 1/T$ is the inverse temperature parameter. and $\mathcal{E}(x)$ is an energy function or Hamiltonian. Z_β is a normalization constant, known as the *partition function*. We are interested in drawing samples from this density, π_β . Due to the size of the configuration space, calculating Z_β directly is impractical. For this reason, a family of Markov-Chain Monte-Carlo (MCMC) algorithms have been developed [8, 17], where Z_β is not needed. In what follows, we will consider the Gibbs sampler [8], but the approach generalizes to other sampling algorithms [6, 8, 17].

In addition to a MCMC sampling algorithm, simulated annealing requires a *cooling schedule*, $\{T_n\}$, or sequence of non-negative values for the temperature parameter. As the name suggests, this may be a strictly decreasing sequence, but this is not necessary. While there are convergence results for *logarithmic* cooling, in practice other schedules are used, for

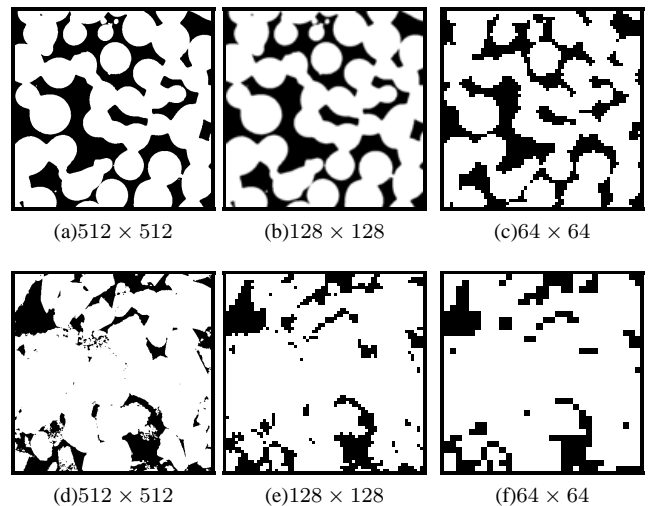


FIG. 2: Lightly fused glass spheres (top row) and Berea sandstone (bottom row) at full resolution and two subsamplings.

example a geometric schedule such as:

$$T_{n+1} = \alpha^n T_0, \quad 0 < \alpha < 1 . \quad (2)$$

In this framework, the standard or *flat* (as opposed to hierarchical) annealing algorithm looks like:

Algorithm 1 Simulated Annealing

```

 $k \leftarrow 0$ 
 $X \leftarrow$  initial state
while  $\mathcal{E}(X)$  not converged do
   $\beta \leftarrow 1/T_k$ 
   $X \leftarrow$  apply Gibbs sampler to  $X$ 
   $k \leftarrow k + 1$ 
end while

```

Heuristically then, an image synthesis algorithm is using simulated annealing to draw (approximate) samples from low energy states of the distribution. This is computationally difficult primarily due to a phenomenon often referred to as *critical slowing down* [10]. Intuitively, this is due to the difficulty of building large-scale structures by the cumulative effects of local interactions. For this reason, even with relatively simple energy functions, a simulated annealing approach may be too expensive. This motivates a multiscale approach, since at coarser scales, large structures become local, or at least the number of local interactions needed is greatly reduced. Figure 2 illustrates the way local (to a pixel) neighbourhoods look quite different at different scales. Consider the relative likelihood of homogeneous white (or black) regions at 512×512 scale, compared with 64×64 (see Figure 2). For example, the neighborhood local to a given pixel is much more often homogeneous in the high resolution images (a) and (d), than in the coarser (c) and (f) (where rescaling has made individual pixels easily discernible).

III. HIERARCHICAL ANNEALING

We propose attacking this problem by use of a hierarchy of scales. The construction of this hierarchy comes from two key ideas. Firstly, there is a natural way to rescale our problem. Secondly, there is a relationship between temperature and characteristic scales of structure in the field.

To expand upon the latter point: Clearly there is no absolute stability of structures under MCMC sampling. However, structures of particular scales are metastable for particular temperature ranges. This is strongly related to the idea of *critical slowing down*, and its relation to the local nature of interactions. To wit, construction or deconstruction of structures beyond the local neighborhood structure of the field can require energetically non-favorable events, which occur only with a certain probability (i.e. transition probabilities in the Markov chain). The larger the extent of these structures, the more consecutive such events may be needed, leading (roughly speaking) to an ever decreasing product of probabilities. Hence large structures take a long time to build (they may be easier to destroy, by way of multiple locations needing only one energetically unfavorable state change). A high enough value of the temperature parameter will simply destroy all structure in the field. Equally clearly, very low temperatures result in near gradient-descent behavior, which will freeze structures in a local minimum energy configuration. As it turns out, analyzing the effect of various cooling schedules is difficult [6, 8, 30]

In considering a hierarchical approach, we want to concentrate on particular scales of structure at particular levels of the hierarchy. For appropriate temperature ranges we expect the following *relative to a particular scale*:

- Larger scale is ‘frozen’ (metastable)
- Current (or medium) scale tends to be ‘slushy’ at characteristic temperatures
- Smaller scale is rapidly changing.

This is borne out empirically.

These ideas taken together suggest a natural hierarchical approach. To take advantage of these observations, we construct a hierarchical approach that will concentrate, at each level of the hierarchy, only on the medium scale structure, leaving the large scale structure intact (or at least not vary it inconsistently). We are not concerned about small scale structure as it is transient anyway. Small structure becomes single or sub-pixel, while the current scale of interest is practically attainable with local interactions, not requiring large numbers of energetically unfavorable events. Algorithm 2 shows this process.

IV. MODELS/ENERGY FUNCTIONS

The purpose of this work is to describe the computational benefits made possible by using a hierarchical approach to simulated annealing. As such, discussion of the relative merits

Algorithm 2 Hierarchical Annealing

```

k ← 0
X ← initial state at coarse resolution
for scale s from coarsest to finest do
  while  $\mathcal{E}^s(X_s)$  not converged do
     $\beta \leftarrow 1/T_k$ 
     $X_s \leftarrow$  apply Gibbs sampler to  $X_s$ 
    k ← k + 1
  end while
   $X_{s-1} \leftarrow P_{s-1}(X_s)$  {project to next finer resolution}
end for

```

of particular models is eschewed. Rather, we present results on common models found in the appropriate literature, with little comment on efficacy or verification.

In particular, there are several components of energy functions that have been used [15, 31, 32] in related approaches, and we demonstrate how the increased performance of the HSA approach improves results with these models.

In general, our energy/cost functions will be made of one or more components. In the hierarchical case, these energy functions will exist for every scale s . Since we can look at separate scales, and also mixtures of these models, the general formulation will be

$$\mathcal{E}^s(x) = \sum_i c_i \mathcal{E}_i^s(x) \quad c_i > 0 \forall i . \quad (3)$$

Here for each scale s the energy \mathcal{E}^s of a particular image x is given as weighted (by coefficients c_i) sum of component energies \mathcal{E}_i^s .

Particular components of interest would be [31–33]:

- one-point correlation function
- two-point correlation function
- chord-length distribution
- lineal path distribution
- “pore size distribution”

In this work we use a method of targeting of mean distributions such as described in [31, 33] Note that in principle a modelling approach may seek to address each scale in (3) separately. This hierarchy allows approaches that are not possible with a single scale algorithm.

V. EXPERIMENTS

A. Synthetic Data

Physical porous media samples tend to have complicated morphology, and it can be difficult to evaluate the performance of a sampling algorithm (for recent approaches, see for example, [3]). In addition to such data, then, it is informative to construct synthetic data to emphasize the benefits of a hierarchical approach.

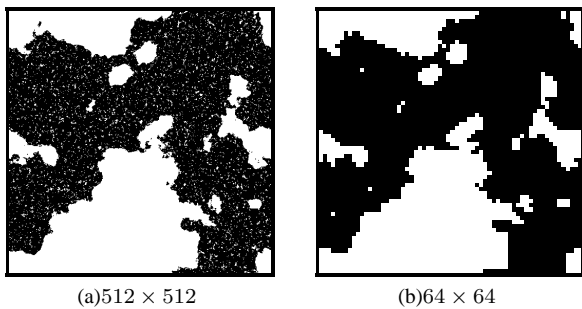


FIG. 3: GRF data generated with two characteristic scales, as shown in a). A strong bias toward black pixels in the shorter length scale GRF has the effect that after several rescalings, the coarse resolution images such as b) are much simpler.

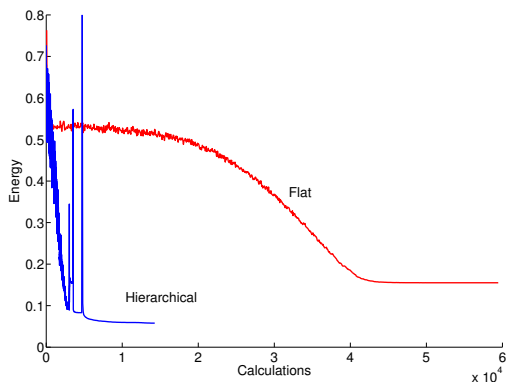


FIG. 4: Convergence flat (red) and hierarchical (blue) annealing for GRF data set. Note spikes in HSA profile due to projection.

First, we consider a set of 300 images generated by means of two Gaussian random fields (GRF)s (for ease of sampling), and chosen to exhibit two characteristic length scales. Figure 3 shows an example of this data set, which allows us to concentrate on two characteristic length scales and on a morphology simpler than may be found in some physical samples. This set is particularly illustrative of the difficulty in convergence of *flat annealing*. Intuitively, this is easy to see in the evaluation of chord-length distributions. At the highest resolution, there are small isolated chords, some small chords on the edges of large features, and longer chords comprising large features. In the annealing algorithm, moving between isolated small chords through isolated medium length chords to eventually collate into larger structures is not energetically favorable, so we have *critical slowing down* as structure begins to emerge. By comparison, coarse levels of the hierarchical annealing do not have any small isolated chords, so we may expect convergence to be quicker. Indeed, empirical results support this conjecture. Figure 4 compares flat and hierarchical sampling runs on a log-log plot of energy vs. computations. The energy ‘spikes’ in the hierarchical annealing curve are due to projection. Immediately after projection, local configurations are high energy due to artifacts of the projection. Since these high energies are due to local configurations, they

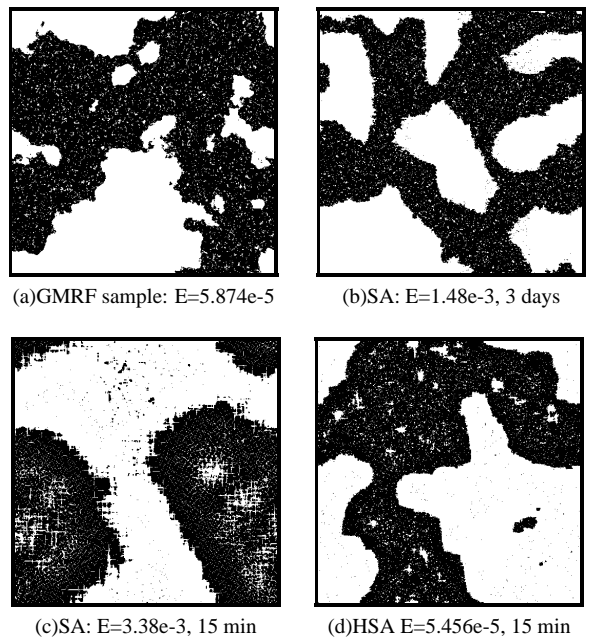


FIG. 5: GRF training data. Each panel gives the final energy, E , and approximate runtime (on a 3Ghz Pentium IV class machine). Shown are a) example training data, b) ‘best case’ sample from SA with very slow geometric cooling c) sample from SA with equivalent computation to the hierarchical case, and finally d) sample from HSA method. Model used was twopoint probability and both white and black phase chord-length distributions. Images are 512×512 pixels.

are easily remedied and energy levels immediately drop as the sampling algorithm progresses.

Figure 5 shows 512×512 images sampled from this model by three methods: the best ‘flat’ SA result allowing about 3 days computation, the best HSA result, taking about 15 minutes, and the best SA we could do (i.e. with a different cooling schedule) in the same number of computations as the HSA sample. As can be seen here, and in a ‘zoom’ view given by Figure 6, the complex morphology is not represented in the SA samples. The long-run result lacks medium size structures, and the fast SA sample is very poor. The HSA result, while clearly less than perfect from a modeling point of view, shows both visually and by final energy a much better result.

B. Computational Benefits

Separate from issues of convergence (analysis of which is difficult for non-logarithmic cooling schedules, and more so where multiple scales are concerned), there are clear sources of expected computational benefit from the HSA approach. At each level of the hierarchy, we are running a Gibbs-type sampler in a smaller configuration space than at the following levels. In the cases described here, each level in the hierarchy reduces the image size by a factor of four (in 3D the gain is much larger, of course), so we have a geometric reduction in the size of the configuration space. Beyond this sim-

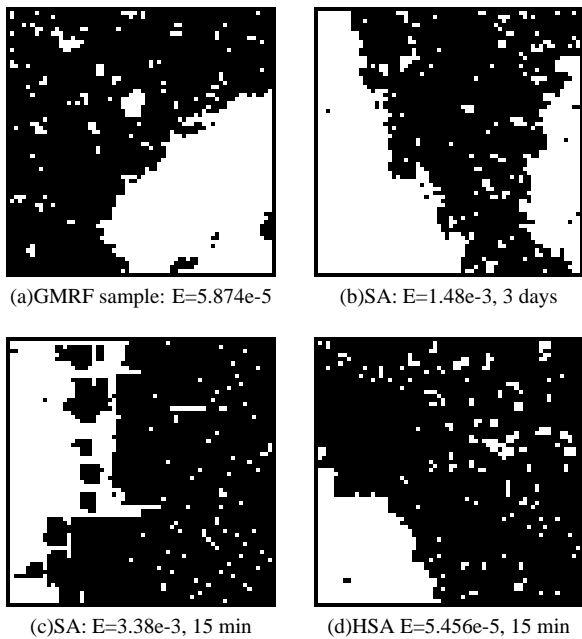


FIG. 6: ‘zoom’ views of images shown in Fig 5

ple reduction, there are data-dependent benefits. Since large scale structures are built by local interactions, the probability of constructing something when the intermediate steps are not energetically favorable is reduced as the number of steps increases (i.e. the product of the probabilities of individual steps). In the hierarchical approach, large structures are put together *with fewer intermediate steps* at a coarser resolution. As this is data dependent, it is difficult to quantify, however the less probable the intermediate steps (in some sense, the more *critical slowing down* experienced) the more it will benefit from a hierarchy.

Evidence of both of these effects was already presented in Figure 4 for our synthetic data. Figure 7 shows the results of many hierarchical runs with a simple parameterization on the cooling schedule. In these simulations, the data set was Berea sandstone, and the model was chord-length distributions in both phases. It is important to note that the parameterization allowed for poor choices of cooling schedule (i.e., that would allow high enough temperatures to tear apart structure after projecting to a high resolution), and these paths are especially evident at the top-right of the ensemble. Many parameterizations allow for very good performance, as evidenced by Figure 8. This figure compares several HSA results, to geometric cooling schedules (2) for flat simulated annealing at the highest resolution but with various values for the parameter α . As expected, increasing α improves the final energy at the cost of more computations. Both figures are presented with log-log scales, so demonstrate a computation vs. energy gain of more than an order of magnitude.

As noted in the previous section, an interesting demonstration of the slow convergence of some models is an energy function made up of both positive (white) and negative (black) chord-length distributions. When attempting to build large

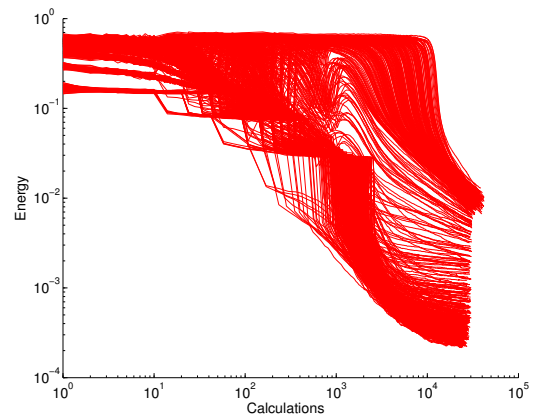


FIG. 7: Energy vs. Computation for many parameterizations of a simple chord-length model.

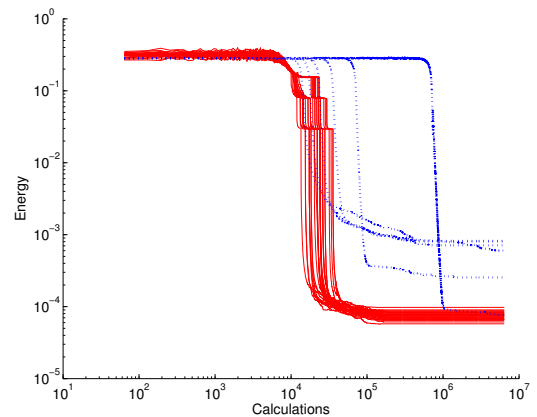


FIG. 8: Energy vs. Computation: several hierarchical annealing runs with flat annealing (dashed lines) for various cooling schedules (increasing α trades more computations for better final energy).

scale structures, such as in our GRF data set, there is very little energy difference made by any intermediate step, as in some sense the white and black chord distributions are at odds, hence very slow convergence results. While this is definitely *not* a good model to capture the morphology in question, it is interesting that even allowing many days, flat annealing will not converge at all usefully, while hierarchical-annealing generates large scale structure in a few minutes. Figure 9 demonstrates this.

C. Physical Data

While empirical results on the synthetic data described in the previous section is valuable, it is of course of interest to apply the approach to real data. It is worth re-iterating that the purpose of this current work is *not* to address modelling issues in the problem domain. For this reason validation of resultant images is difficult, at least in an absolute sense. While subtle issues of validation are beyond the scope of the paper, in comparison to flat annealing, improvements can be *extremely*

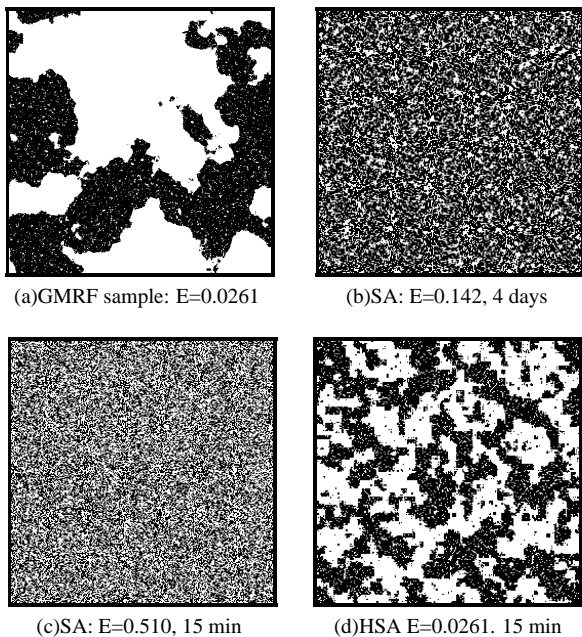


FIG. 9: Similar to Figure 5, these panels show results for the (more difficult) case where the energy function is a mix only of white and black phase chordlength.

clear.

Figure 10 shows the same computational methods as Figure 9 but with a data set of lightly fused glass beads. Note again the complete failure of convergence for the flat annealing cases.

In comparison, Figure 11 shows similar samples, but for a more realistic model, of chord-length distribution and two-point correlation. This is *still* not a sufficient model to capture the morphology of the training set. We can see, though, that the samples are drawn from a class of images with chord-length distributions that are strongly in agreement with the mean chord-length of the training set, as Figure 12 demonstrates. So we see that the process under the HSA algorithm is converging to something with reasonably low energy under this model. Of course, this in no way addresses the question of whether or not the mean distribution is the correct way to model these images.

VI. CONCLUSIONS

We have demonstrated the computational benefit of a hierarchical approach to simulated annealing in the computationally expensive approach of pure synthesis (i.e. sampling) from low temperature Gibbs distributions (1). This approach now allows researchers to attempt more difficult synthesis problems, on large images with multiple natural length scales. Clearly, in such an approach, there is a modeling component not addressed in the current work. While some comments relevant to modeling in such a hierarchy have been made, this aspect is the subject of another paper. As an example, though,

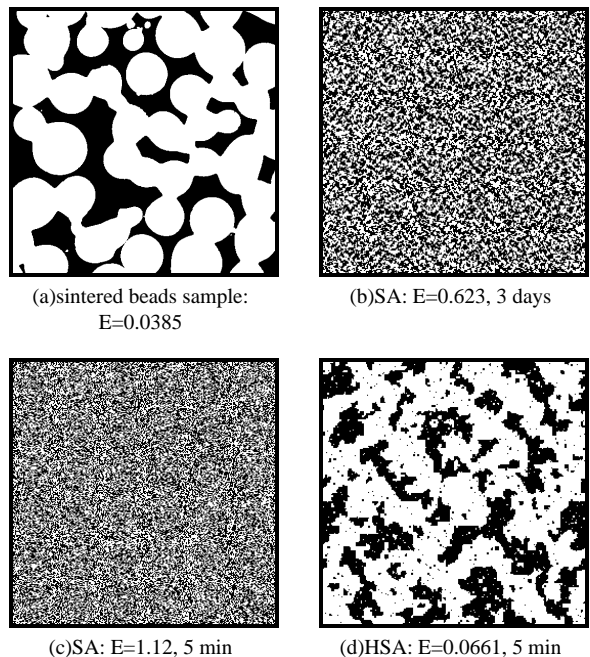


FIG. 10: Sintered beads data set. Again, each panel gives the final energy, E , and approximate runtime. Shown are a) example training data, b) sample from SA with very slow geometric cooling c) sample from SA with equivalent computation to the hierarchical case but with enforced volume fraction (to the mean of the training set), and finally d) sample from HSA method described herein. Model is (cf Figure 9) both white and black phase chord-length distributions. Images are 256×256 pixels.

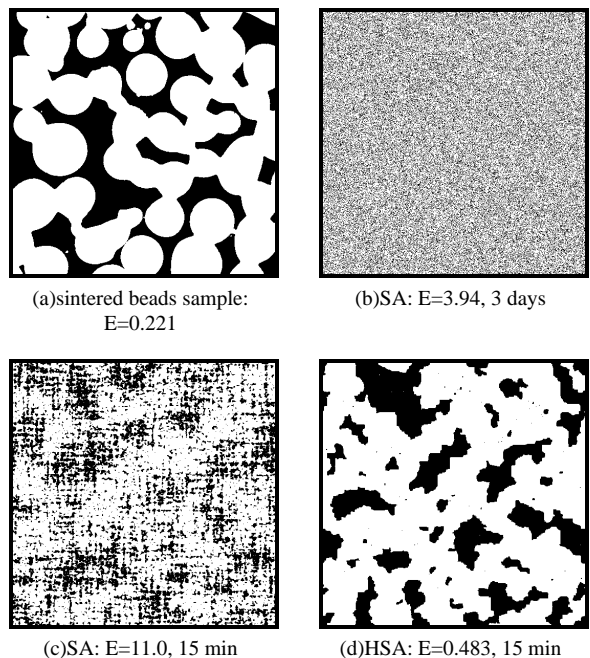


FIG. 11: Sintered beads data set with a slightly more realistic energy function, the mixture of twopoint probability and chordlength distribution. In this case the images are 512×512 .

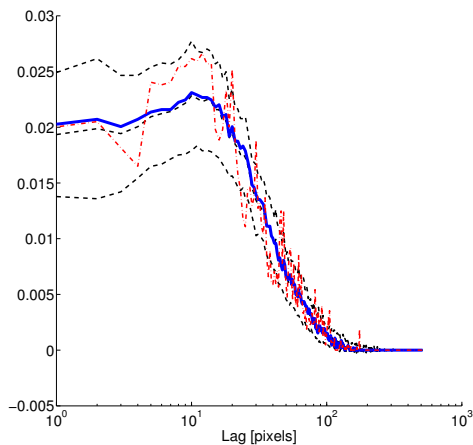


FIG. 12: Chordlength distributions for spheres data set (shown in Fig 11). The dashed line is mean chord-length distribution over training set, and dotted lines give one standard deviation. The solid line is final distribution of an HSA sample, while dot-dash line shows a typical sample from the training set.

Figure 13 shows preliminary results of reconstruction based on HSA of local (to a neighborhood) distributions of pixels, and chordlength distribution. This reconstruction was done for a 8192×8192 image, in approximately 4 days of computation time. The left column of Figure 13 shows training data at -a full resolution, and two sub-images -b (1024×1024) and -c (128×128), the sub-image regions as indicated on previous resolution. The right column shows similar regions for our reconstruction. Finally, Figure 14 shows autocorrelation for these two images, showing good agreement.

Two obvious extensions of this work are to apply it to three-dimensional data, and to further address modelling questions. Both of these directions are currently being pursued. Furthermore, the question of validating synthetic images for the relevant applications is important.

-
- [1] P.M. Adler, C.G. Jacquin, and J.A. Quiblier, *Flow in simulated porous media*, International Journal of Multiphase Flow **16** (1990), no. 4, 691–712.
- [2] P.M. Adler, C.G. Jacquin, and J.-F. Thovert, *The formation factor of reconstructed porous media*, Water Resources Research **28** (1992), no. 6, 1571–1576.
- [3] C.H. Arns, M.A. Knackstedt, and Mecke K. R., *Characterisation of irregular spatial structures by parallel sets and integral geometric measures*, Colloids And Surfaces A-Physicochemical And Engineering Aspects **24** (2004), 351–372.
- [4] S. Bekri, J. Howard, J. Muller, and P.M. Adler, *Electrical resistivity index in multiphase flow through porous media*, Transport in Porous Media **51** (2003), no. 1, 41–65.
- [5] N.F. Berk, *Scattering properties of a model bicontinuous structure with a well defined length scale*, Physical Review Letters **58** (1987), no. 25, 2718–2721.
- [6] P. Brémaud, *Markov chains: Gibbs fields, monte carlo simulation, and queues*, Springer, 1998.
- [7] E.J. Garboczi and A.R. Day, *An algorithm for computing the effective linear elastic properties of heterogeneous materials: Three-dimensional results for composites with equal phase poisson ratios*, Journal of the Mechanics and Physics of Solids **43** (1995), no. 9, 1349–1503.
- [8] S. Geman and D. Geman, *Stochastic relaxation, Gibbs distributions, and the Bayesian restoration of images*, IEEE Transactions on Pattern Analysis and Machine Intelligence **6** (1984), 721–741.
- [9] B. Gidas, *A renormalization group approach to image processing problems*, IEEE Transactions on Pattern Analysis and Machine Intelligence **11** (1989), no. 2, 164–180.
- [10] J. Goodman and A. Sokal, *Multigrid monte carlo method. conceptual foundations*, Physical Review D **40** (1989), no. 6, 2035–2071.
- [11] M.A. Ioannidis, M.J. Kwiciczen, and I. Chatzis, *Electrical conductivity and percolation aspects of statistically homogeneous porous media*, Transport in Porous Media **29** (1997), no. 1, 61–83.
- [12] M.E. Kainourgiakis, E.S. Kikkinides, G.Ch. Charalambopoulou, and A.K. Stubos, *Simulated annealing as a method for the determination of the spatial distribution of a condensable adsorbate in mesoporous materials*, Langmuir **19** (2003), no. 8, 3333–3337.
- [13] P. Levitz, *Off-lattice reconstruction of porous media: critical evaluation, geometrical confinement and molecular transport*, Advances in Colloid and Interface Science **77** (1998), 71–106.
- [14] Z. Liang, M.A. Ioannidis, and I. Chatzis, *Permeability and electrical conductivity of porous media from 3d stochastic replicas of the microstructure*, Chemical Engineering Science **55** (2000), no. 22, 5247–5262.
- [15] Z. Liang, M.A. Ioannidis, and I. Chatzis, *Reconstruction of 3d porous media using simulated annealing*, Computational Methods in Water Resources XIII (Balkema, Rotterdam) (Bentley et al., ed.), 2000.
- [16] F.S. Magnani, P.C. Philippi, Z.R. Liang, and C.P. Fernandes, *Modelling two-phase equilibrium in three-dimensional porous microstructures*, International Journal of Multiphase Flow **26** (2000), no. 1, 99–123.
- [17] N. Metropolis, A. W. Rosenbluth, M. N. Rosenbluth, A. H. Teller, and E. Teller, *Equation of state calculations by fast computing machines*, Journal of Chemical Physics **21** (1953), 1087–1092.
- [18] A. Moctezuma-Berthier, O. Vizika, and P.M. Adler, *Macroscopic conductivity of vugular porous media*, Transport in Porous Media **49** (2002), no. 3, 313–359.
- [19] A. Moctezuma-Berthier, O. Vizika, J.F. Thovert, and P.M. Adler, *One- and two-phase permeabilities of vugular porous media*, Transport in Porous Media **56** (2004), no. 2, 225–244.
- [20] S. Olayinka and M.A. Ioannidis, *Time-dependent diffusion and surface-enhanced relaxation in stochastic replicas of porous rock*, Transport in Porous Media **54** (2004), no. 3, 273–295.
- [21] A.P. Radlinski, M.A. Ioannidis, A.L. Hinde, M. Hainbuchner,

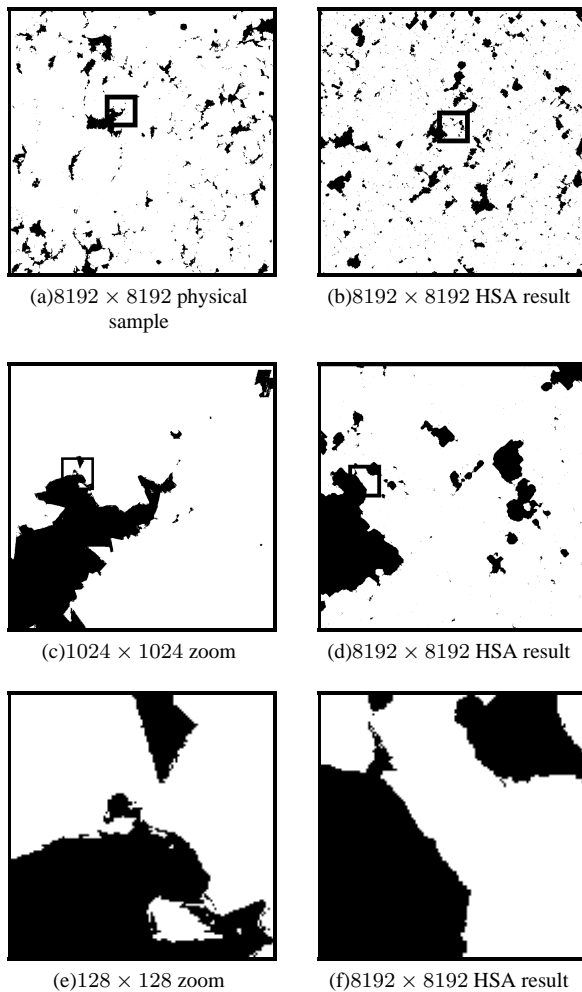


FIG. 13: High-resolution image of vuggy carbonate rock (1.87 micron/pixel) showing structure at multiple scales (left column) and HSA sample (right column). Energy function is based on local neighborhood structure and chordlength distributions. The reconstruction took approximately 4 days, with a final energy of $E=2.85e-4$ (the original image has energy of $4.44e-6$).

H. Rauch M. Baron, and S.R. Kline, *Angstrom-to-millimeter characterization of sedimentary rock microstructure*, Journal of Colloid and Interface Science **274** (2004), no. 2, 607–612.

- [22] A.P. Roberts, *Statistical reconstruction of three-dimensional porous media from two-dimensional images*, Physical Review E **56** (1997), no. 3, 3203–3212.
- [23] A.P. Roberts and E.J. Garboczi, *Computation of the linear elastic properties of random porous materials with a wide variety of microstructure*, Proceedings of the Royal Society of London **458** (2002), no. 2021, 1033–1054.

- [24] A.P. Roberts and M.A. Knackstedt, *Structure-property correlations in model composite materials*, Physical Review E **54** (1996), no. 3, 2318–2328.
- [25] A.P. Roberts and M. Teubner, *Transport properties of heterogeneous materials derived from gaussian random fields: Bounds and simulation*, Physical Review E **51** (1995), no. 5, 4141–4154.
- [26] M.G. Rozman and M. Utz, *Efficient reconstruction of multi-*

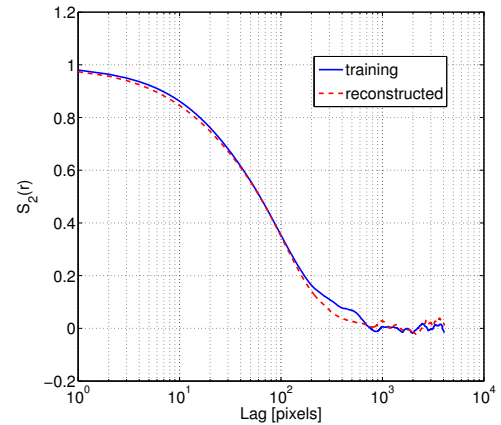


FIG. 14: Plots of the autocorrelation function $S_2(r)$ for both training and reconstructed images shown in Figure 13. Although autocorrelation is not directly part of the energy function used, agreement is very good.

phase morphologies from correlation functions, Physical Review E **63** (2001), no. 066701.

- [27] M. Sahimi, *Flow phenomena in rocks: from continuum models to fractals, percolation, cellular automata, and simulated annealing*, Reviews of Modern Physics **65** (1993), no. 4, 1393–1534.
- [28] M. Singh and K.K. Mohanty, *Permeability of spatially correlated porous media*, Chemical Engineering Science **55** (2000), no. 22, 5393–5403.
- [29] P. Spanne, J.F. Thovert, C.J. Jacquin, W.B. Lindquist, K.W. Jones, , and P.M. Adler, *Synchrotron computed microtomography of porous media: Topology and transports*, Physical Review Letters **73** (1994), no. 14, 2001–2004.
- [30] H. Szu and R. Hartley, *Fast simulated annealing*, Physics Letters A **122** (1987), 157–162.
- [31] M.S. Talukdar, O. Torsaeter, and M.A. Ioannidis, *Stochastic reconstruction of particulate media from two-dimensional images*, Journal of Colloid and Interface Science **248** (2002), no. 2, 419–428.
- [32] S. Torquato, *Random heterogeneous materials: Microstructure and macroscopic properties*, Springer-Verlag, New York, 2001.
- [33] C.L.Y. Yeong and S. Torquato, *Reconstructing random media*, Physical Review E **57** (1998), 495–506.